DOI: https://doi.org/10.2138/am-2018-6363

Kuliginite, a new hydroxychloride mineral from the Udachnaya kimberlite pipe, Yakutia: Implications for low-temperature hydrothermal alteration of the kimberlites. Revision 4

Denis S. Mikhailenko[a,*], Andrey V. Korsakov[a], Sergey V. Rashchenko[a,b], Yurii V. Seryotkin[a,b], Dmitriy I. Belakovskiy[c], Alexander V. Golovin[a]

[a] *V.S. Sobolev Institute of Geology and Mineralogy of the Siberian Branch of the RAS, 3, Ac. Koptyuga ave., Novosibirsk 630090, Russian Federation*
[b] *Novosibirsk State University, 1 Pirogova Street, 630090 Novosibirsk, Russia*
[c] *Fersman Mineralogical Museum, Russian Academy of Sciences, Leninskiy Prospekt 18 korp. 2, Moscow 119071, Russia*

Abstract

Kuliginite is a new iron-magnesium hydroxychloride mineral with the ideal formula $Fe_3Mg(OH)_6Cl_2$ from the Udachnaya East kimberlite, Yakutia, Russia. It occurs as green prismatic-bipyramidal crystals (0.2-0.5 mm) and fills cavities and veins in several units of kimberlites together with iowaite, gypsum, calcite, halite, barite, and celestine. It is trigonal, with $R\bar{3}$ space group. The spinel-like crystal structure of kuliginite is also typical for a number of copper minerals of the atacamite group with common formula $Cu_3M(OH)_6Cl_2$; kuliginite can be regarded as a Fe^{2+} analogue of tondiite ($Cu_3Mg(OH)_6Cl_2$).

The occurrence of the kuliginite + iowaite + gypsum assemblage has implications for the interpretation of low-temperature (below 100 °C) hydrothermal processes and alteration of kimberlite by hydrothermal fluids/brines, as well as for transport of metals in Cl-bearing solutions. This secondary hydrothermal mineral assemblage formed much later than the kimberlite groundmass minerals. Kuliginite contains inclusions of iowaite indicating their simultaneous

*Corresponding author
Email address: pazilovdenis@igm.nsc.ru (Denis S. Mikhailenko)

crystallization.

Keywords: New mineral, Kuliginite, Crystal structure, Kimberlite, Atacamite group, Hydroxychloride

---

Introduction

The Paleozoic Udachnaya kimberlite pipe is the world's largest diamond deposit located in the Yakutsk diamond province in the central Siberian craton. It has a complex structure (Kharkiv et al., 1998), with several distinct "volcanoclastic units" and "coherent" kimberlite in each (Fig. 1), according to the modern model (Smith et al., 2013).

Na-K-Cl-bearing minerals were found in various assemblages from different units of the Udachnaya East kimberlite, but the source of Na and Cl in these units remains poorly constrained. Melt inclusion studies (Golovin et al., 2003, 2007, 2017; Kamenetsky et al., 2004, 2006, 2007b, 2009, 2014; Mernagh et al., 2011), as well as Sr, Nd, and Pb isotopes (Maas et al., 2005; Kamenetsky et al., 2009, 2014) and sulfur isotope data (Kitayama et al., 2017) on the Udachnaya-East rocks provide solid proofs for magmatic mantle origin of the Na-K-Cl component in two non-serpentinized ultrafresh units of the Udachnaya East kimberlite. Thus, the discovery of these two compositionally unusual units offers a unique opportunity to study the composition and evolution of kimberlitic magma (Golovin et al., 2017; Kamenetsky et al., 2008, 2012, 2014; Kitayama et al., 2017). On the other hand, some authors argue that any assemblage with chlorides larger than 1 cm in any unit of the Udachnaya East kimberlite from the depths of 410-640 m may be evaporatic or xenoliths coming from the host sediments (Kopylova et al., 2016).

This paper presents new data on mineral assemblages containing chlorides in voids from several types of kimberlites originated at the depths of 560-640 m in the Udachnaya East pipe, where a new hydroxychloride mineral, kuliginite, was found. Kuliginite is a new iron-magnesium hydroxychloride (IMA 2016-049) that belongs to the atacamite group (Hålenius et al., 2016) and was named

after Sergey Semenovich Kuligin, Russian geologist and researcher (07.09.1961-12.05.2014), who for years studied Yakutian kimberlites and xenoliths and alluvial diamond deposits all over Yakutia in search for unknown kimberlite pipes. S. S. Kuligin, together with his colleagues from the Sobolev Institute of Geology and Mineralogy (IGM, Novosibirsk, Russia), discovered the Nicka diamondiferous placer along the Tyung River (Yakutia). The holotype sample of kimberlite with abundant kuliginite is stored in the collection of the Central Siberian Geological Museum of IGM under the number VI-53/1.

Analytical techniques

Mineral chemistry of kuliginite (40 chemical analyses, Table 1), iowaite, celestine and calcite were determined in IGM using a JEOL JXA-8100 electron microprobe operated at 20 kV acceleration voltage, 5 μm beam diameter, 50 nA focused beam current and 20-30 s counting time; TESCAN MIRA 3 LMU JSM 6510LV equipped with an Oxford Instruments INCA energy-dispersive detector was used for chemical mapping at the operating conditions 20 kV, 1 nA, with an interval of 0.78 s for each spot.

Raman spectra in the range from 50 to 4000 cm^{-1} were collected with a Horiba Jobin Yvon LabRam HR800 Laser Raman spectrometer, using a 532 nm laser, at 15 mW (spot size of about 0.8 μm) coupled with an Olympus microscope with an LMPLFLN100x long-working distance objective (focal length 640 mm).

A 0.56×0.37×0.08 mm^3 single crystal of kuliginite was selected for single-crystal X-ray diffraction using a polarizing microscope. X-ray diffraction data were collected on an Oxford Diffraction Gemini R Ultra single-crystal diffractometer (CCD-detector, graphite-monochromatized Mo $K\alpha$ radiation) using an ω-scan technique with the scan width of 1° per frame. Data reduction with numeric and empirical absorption corrections was performed using Rigaku Oxford Diffraction CrysAlis^{Pro} software. Space group $R\bar{3}$ was selected on the basis of R_{int} (4.18 % for $R\bar{3}$, 7.36 % for $R\bar{3}m$), the choice was then supported by analysis of wR values (see below). JANA 2006 software (Petrícek et al., 2014) including

This is a preprint, the final version is subject to change, of the American Mineralogist (MSA)
Cite as Authors (Year) Title. American Mineralogist, in press.
DOI: https://doi.org/10.2138/am-2018-6363

SUPERFLIP program (Palatinus and Chapuis, 2007) was used for structure solution and refinement. Coordinates of all atomic positions except hydrogen (M1, M2, O1, and Cl1) were obtained from charge flipping. Coordinates of the remaining hydrogen position (H1) were extracted from a Fourier difference map. Anisotropic displacement parameters were refined for all atomic positions except isotropically refined hydrogen. A refinement of Fe/Mg proportion in M1 and M2 sites resulted in $Fe_{0.97}Mg_{0.03}$ occupancy of M1 site, and $Mg_{0.85}Fe_{0.15}$ occupancy of M2 site, giving the formula $Fe_{3.04}Mg_{0.96}(OH)_6Cl_2$, consistent the formula derived from the chemical analyses, $Fe_{2.98}Mn_{0.11}Mg_{0.91}(OH)_6Cl_2$ (note that Fe and Mn cannot be separated on the basis of X-ray diffraction). Bond-valence calculations (Table 2) confirm that Fe^{2+} and Mn^{2+} should preferentially occupy M1 site, and Mg^{2+} – M2 site.

Crystal data, data collection and structure refinement details are summarized in Table 3; fractional atomic coordinates and isotropic or equivalent isotropic displacement parameters are summarized in Table 4 (see also Supplementary CIF).

A powder X-ray diffraction pattern of kuliginite (Fig. 2) was measured using a DRON diffractometer (Bragg-Brentano geometry, Cu $K\alpha$ radiation). Main diffraction peaks are listed in Table 5.

Geological setting

The Udachnaya kimberlite pipe consists of two kimberlite bodies at the surface: East and West Udachnaya kimberlites (Kharkiv et al., 1998). The Udachnaya-East kimberlite has a U-Pb age of 367±5 Ma, and the age of the West body is in a range of 353-359 Ma (Kinny et al., 1997), but its separate units (possibly, phases) have never been dated (Fig. 1). As shown by $^{40}Ar/^{39}Ar$ dating of phlogopite from kelyphitic rims around garnet from Udachnaya East kimberlite pipe (Yudin et al., 2011), the kimberlite magma of the western body intruded later and affected thermally the already formed kimberlites of eastern pipe. The Udachnaya kimberlite intruded Lower Ordovician (exposed on the surface)

and Middle and Upper Cambrian (obtained from drilling) dolomite, limestone, marl, mudrocks, siltstone, and sandstone and encloses xenoliths of limestone and dolomite with minor amounts of clayey and sandy material, as well as marl and siltstone, no younger than Devonian (Davis et al., 1980; Brakhfogel, 1984; Kinny et al., 1997).

There are several units of kimberlites within the Udachnaya system (Fig. 1; Kharkiv et al. (1998)). The western body is strongly serpentinized all along the exposed depth of 1400 m (Kharkiv et al., 1998), while the eastern body comprises two non-serpentinized units (Fig. 1, units 9a and 10), at depths below 370 m and at least four units serpentinized to different degrees, with different contents of olivine and olivine/serpentine ratios (Fig. 1).

Volcanoclastic and coherent non-serpentinized kimberlites from the depths 410-500 m (Fig. 1, units 9a and 10) contain chlorides, alkali carbonates, and alkali sulfates and sulfides in the groundmass (Kamenetsky et al., 2008, 2009, 2012, 2014; d′Eyrames et al., 2017), as well as the so-called chloride and chloride-carbonate nodules reaching 30 cm in diameter, which are uncommon in other kimberlites worldwide. The chloride nodules are composed mainly of halite and sylvite, while the chloride-carbonate ones consist of chlorides, calcite, and a series of Na-Ca carbonates (shortite $Na_2Ca_2(CO_3)_3$, nyerereite $(Na,K)_2Ca(CO_3,)_2$ and northupite – $Na_3Mg(CO_3)_2Cl$ and a minor amount of aphthitalite – $K_3Na(SO_4)_2$ (Kamenetsky et al., 2006, 2007a, 2014).

The host sediments include several aquifers. One deep aquifer system has its top at 510 m below the surface and stores strong brines of a calcium chloride composition and water-bearing kimberlite zones (Drozdov et al., 1989; Alexeev et al., 2007). All kimberlites below 510 m contain neither chloride and chloride-carbonate nodules nor assemblages of chlorides with alkali carbonates and sulfates in the groundmass, and all units of the Udachnaya East kimberlite within the 510-640 m depths are more or less strongly serpentinized. At the same time, both volcaniclastic and coherent kimberlites between 560 and 640 m include later mineral assemblages with halite and sylvite which fill veins, fractures and voids and can reach tens of cm in size (Fig. 3).

This is a preprint, the final version is subject to change, of the American Mineralogist (MSA)
Cite as Authors (Year) Title. American Mineralogist, in press.
DOI: https://doi.org/10.2138/am-2018-6363

Occurrence and mineral associations of kuliginite

Kuliginite and iowaite, together with other minerals, were found in cavities or veins in weakly serpentinized volcaniclastic and coherent kimberlites of the Udachnaya East pipe below 560 m. The amount of xenolithic material from the sediment host is moderate in volcaniclastic kimberlite (∼15 vol. %, Fig. 3), which constitutes a separate unit in the central part of the East pipe below 510 m (Fig. 1, units 9b), and low in coherent kimberlite (∼5 vol. %, Fig. 4a, unit 10 in Fig. 1) which is a dike in xenolith-rich (∼50 vol. %) volcaniclastic kimberlite (unit 7 in Fig. 1) exposed at the depth about 560 m in the southwestern part of the Udachnaya East kimberlite.

Kuliginite was identified as euhedral prismatic-bipyramidal crystals (0.2-0.5 mm) (Fig. 4b) in aggregates with iowaite, calcite, as inclusions in halite (Fig. 3, 4), and also together with gypsum and barite (Fig. 3, 5b). Kuliginite crystals are green (Fig. 3) and some are coated by a red rust-like phase as a result of Fe(II) oxidation (Fig. 3a-b). The following crystallization sequence of minerals was observed: serpentine $\longrightarrow$ calcite $\longrightarrow$ kuliginite + iowaite + halite + barite + calcite + gypsum $\longrightarrow$ halite (Fig. 6). Note that abundant kuliginite and iowaite inclusions occur in centers of halite lenses or veins in kimberlite. Both kuliginite and iowaite crystals become coarser from toward the vein center. Kuliginite slowly dissolves in H_2O at room temperature, but oxidizes very fast upon interaction with atmospheric water even at ambient humidity. The empirical formula, based on four cations per formula unit (pfu), is $(Fe_{2.98}Mn_{0.02})(Mg_{0.91}Mn_{0.09})(OH_{5.95}F_{0.03}Cl_{0.02})Cl_2$. The ideal end-member formula is $Fe_3Mg(OH)_6Cl_2$.

Coarse (2-3 cm), dark green pseudohexagonal iowaite crystals in the Udachnaya kimberlite are intergrown with elongate prismatic crystals of gypsum and kuliginite or enclosed in halite and gypsum (Fig. 3, 7). The crystals are free from features of dissolution. Some iowaite ($Mg_6Fe^{3+}_2(OH)_{16}Cl_2{\cdot}4H_2O$) has transformed into brown-gilded pyroaurite ($Mg_2Fe_2CO_3(OH)_6{\cdot}4H_2O$) under

sunlight (Fig. 3d). The Udachnaya iowaite markedly differs in mineral chemistry from its synthetic counterparts (Frost et al., 2005) and natural analogs (Braithwaite et al., 1994). The chemical composition of iowaite is shown in Table 6.

Elongate prisms of gypsum (up to 20 cm long) bear abundant visible inclusions of other minerals (iowaite, halite, etc.). Gypsum is either intergrown with or enclosed in halite (single inclusions), which also hosts anhydrite inclusions with up to 2.3 wt. % SrO.

Massive euhedral crystals of halite, reaching 10 cm grown together with elongate gypsum prisms (Fig. 3a,d; 7a) and enclose gypsum, kuliginite, and celestine. Halite contains minor amounts of impurities, below the detection limit, and H_2O fluid inclusions marked by a Raman peak at 3446 cm^{-1} (Fig. 8b).

Celestine grains are either euhedral or anhedral. Euhedral grains (up to 2.5 cm in size) were identified in a large gypsum crystal (up to 7 cm in size), and anhedral celestines (up to 80-90 μm in size) occur as inclusions in halite. The composition of celestine approaches stoichiometry but many grains contain 9.6 to 13.6 wt. % BaO (Table 6).

Carbonates in the studied mineral assemblage are represented only by calcite (with 0.5-0.7 wt. % SrO) found as inclusions in halite and syngenetic intergrowths with kuliginite.

Physical properties

Kuliginite crystals (0.5 mm) are dark-green and transparent and non-pleochroic in transmitted light. Some grains (or grain parts) are greenish-yellow, obviously due to inclusions of iron oxides or hydroxides produced by alteration. Despite trigonal symmetry, the mineral shows anomalous biaxiality with $2V_{(meas)} = 10(5)^\circ$ (see discussion below). Grain fragments often have somewhat rhombic shape with the acute angle close to 65°. Taking into account that rhombohedral angle of kuliginite unit cell is near 67 degrees, one can suggest imperfect cleavage

This is a preprint, the final version is subject to change, of the American Mineralogist (MSA)
Cite as Authors (Year) Title. American Mineralogist, in press.
DOI: https://doi.org/10.2138/am-2018-6363

on {10-11} main rhombohedron similarly to herbertsmithite and leverettite.

Kuliginite is biaxial (+), $\alpha = 1.709(3)$, $\beta = 1.709(3)$, $\gamma = 1.718$ ($\lambda = 589$ nm)

Dispersion of the optical axis is noticeably, r> ν

The density of kuliginite measured by the sink-float method, using about ten microscopically selected fragments free from inclusions, is 3.13 g/cm^{-3} (D_{calc} = 3.001 g/cm^{-3}); Mohs hardness is 3-3.5.

Crystal structure

The crystal structure of kuliginite has atomic packing similar to spinel structure with vacant tetrahedral sites. Octahedral sites in the kuliginite structure are represented by 'intralayer' M1 site occupied by $Fe_{0.97}Mg_{0.03}$, and 'interlayer' M2 site, occupied by $Mg_{0.85}Fe_{0.15}$. The M1:M2 ratio in the crystal structure is 3:1. The M1 site is coordinated by four hydroxyl groups and two chloride anions in the opposite vertices of a slightly distorted $Fe(OH)_4Cl_2$ octahedron. These $Fe(OH)_4Cl_2$ octahedra form gibbsite-type layers parallel to the (001) plane; the chloride anions appear on the junctions of three such octahedra (Fig. 9a). The M2 site is coordinated by six hydroxyl groups, and links neighboring gibbsite-type layers of M1-centered octahedra through the triple junctions (Fig. 9b-c). The structural formula of the kuliginite is therefore $^{M1}(Fe_{2.89}Mg_{0.11})^{M2}(Mg_{0.85}Fe_{0.15})(OH)_6Cl_2$.

An interesting feature of kuliginite structure is a breaking of possible $R\bar{3}m$ symmetry due to slight (less than 0.1 Å) displacement of oxygen and hydrogen atoms from {110} planes, whereas remaining atomic sites are situated in special positions compatible with $R\bar{3}m$ (Fig. 9d, Table 3). Although the structure can be also solved in the $R\bar{3}m$ space group, the resulting wR factor of 7.12 % (for all reflections) is considerably higher than corresponding value of 4.83 %, obtained for solution in the $R\bar{3}$ space group. An application of Hamilton test (Hamilton, 1965) to these values suggests the correctness of our space group choice within significance level of 0.005.

This is a preprint, the final version is subject to change, of the American Mineralogist (MSA)
Cite as Authors (Year) Title. American Mineralogist, in press.
DOI: https://doi.org/10.2138/am-2018-6363

The chloride anions on the junctions of three M1-centered octahedra also play a role of proton acceptors for three hydroxyl groups of adjacent gibbsite-type ring (Fig. 9d). The resulting O-H···Cl bonds are characterized by distances H···Cl of 2.39(3) Å, O···Cl of 3.2376(12) Å, and angle O-H···Cl of 162(2)°. Such parameters allow classification of these bonds as hydrogen bonds according to a number of dedicated studies (Mascal, 1997; Aullon et al., 1998; Steiner, 1998). Although there is no systematic study how strength of O-H· · ·Cl hydrogen bond affects O-H stretching frequency like that made by Libowitzky (1999) for O-H· · ·O bonding, the observed O-H stretching frequencies of kuliginite (3550-3575 cm^1 - see Fig. 8a and Table 6) correspond to "plateau" on the Libowizky's ν(O-H) / d(O· · ·O) plot, indicating a negligible influence of weak O-H···Cl hydrogen bonding. The observed splitting of O-H stretching frequency into three components (Fig. 8a) most probably corresponds to the Mg-for-Fe substitution in M2 site and presence of Mn in octahedral sites.

Raman spectroscopy

Kuliginite

Unpolarized single-crystal Raman spectra of kuliginite (Fig. 8A) show a band at 445 cm^{-1} which is close to that of synthetic $Fe_2(OH)_3Cl$ and can be attributed to a Fe-O stretching mode, similarly to (Reguer et al., 2007) (Table 6). The Raman bands in the range 3600-3500 cm^{-1} may be attributed to OH hydroxyl stretching vibrations (Fig. 8A).

Iowaite

The Raman spectra of iowaite from our mineral assemblage (Fig. 10) show typical peaks at 524, 279, 437 and 101 cm^{-1} (Frost et al., 2005). One spectrum contains a CO_3 carbonate peak at 1307 cm^{-1}. Other bands are observed for synthetic and natural iowaite at 3545, 3421, 3281, 3058, and 2769 cm^{-1}, which are assigned to the stretching vibrations of interlayer water (Frost et al., 2005).

This is a preprint, the final version is subject to change, of the American Mineralogist (MSA)
Cite as Authors (Year) Title. American Mineralogist, in press.
DOI: https://doi.org/10.2138/am-2018-6363

Discussion

Related minerals

Kuliginite belongs to the atacamite group of hydroxychloride minerals with $M_2(OH)_3Cl$ stoichiometry, where M is a divalent cation (Cu^{2+}, Mg^{2+}, Fe^{2+}, Mn^{2+}, Co^{2+}, Ni^{2+}, Zn^{2+}). The members of atacamite group may be divided into two subgroups: with brucite-like stacking of cation coordination octahedra, and with spinel-like stacking of cation coordination octahedra (Table 7).

The spinel-like trigonal structure of kuliginite is also typical for a number of copper minerals of the atacamite group including herbertsmithite, gillardite, leverettite, tondiite and paratacamites (Table 7). Kuliginite, $Fe_3Mg(OH)_6Cl_2$, herewith, can be regarded as Fe-analogue of tondiite, $Cu_3Mg(OH)_6Cl_2$. The composition of kuliginite is quite similar to that of hibbingite - an orthorhombic $Fe_2(OH)_3Cl$ hydroxychloride, especially if the latter demonstrates a partial $Fe^{2+} \longleftarrow Mg^{2+}$ substitution (Saini-Eidukat et al., 1994). However, the difference in symmetry results in different X-ray diffraction patterns (Fig. 11) allowing the discrimination of these species by means of X-ray diffraction.

An important issue is a relation of kuliginite to atacamite mineral species. On the one hand, amakinite was described as a mineral with $Fe(OH)_2$ idealized composition and brucite-like structure (Kozlov and Levshov, 1962), and herewith by no means related to kuliginite. On the other hand, the reported optical and physical properties, X-ray diffraction (Fig. 11), lattice parameters (a = 6.917(3), b = 14.52(1) A), and cationic composition ($Fe_{2.92}Mg_{0.90}Mn_{0.18}$ normalized per 4 cations) of amakinite too strongly resembles those of kuliginite to be accidental. Taking into account that the crystal structure of amakinite has actually never been determined, and chemical analysis applied in 1962 probably was not able to detect chlorine we conclude that amakinite is closely related to kuliginite. Unfortunately, the holotype of amakinite was reported to be completely decomposed into rust (Dmitriy I. Belakovskiy, Fersman Mineralogical Museum, private communication), so the verification of our hypothesis is impossible.

This is a preprint, the final version is subject to change, of the American Mineralogist (MSA)
Cite as Authors (Year) Title. American Mineralogist, in press.
DOI: https://doi.org/10.2138/am-2018-6363

The mixed occupancy $Mg_{0.85}Fe_{0.15}$ of 'intralayer' cation site in kuliginite also implies the existence of samples close to a Fe-dominant analog of kuliginite with idealized formula $Fe_3Fe(OH)_4Cl_2$. Such a compound with $R\bar{3}m$ space group (a = 6.9594(5), c = 14.7847(12) A) was described among synthetic materials (ICSD-155535), but was not observed among minerals yet.

Formation of the kuliginite mineral assemblages

Kuliginite is a rare phase with optic properties impeding its identification: its biaxiality is inconsistent with its trigonal symmetry observed by X-ray diffraction. Thus, the biaxial behavior must be anomalous. Anomalous optics of uniaxial compounds is relatively common and described in detail by Shtukenberg and Punin (2007). It is often observed in beryl, indialite, osumilite-group minerals, etc., and is usually due to deformation associated with stress during or after crystallization. It might also result from variations of oxidation and/or dehydration degrees in different crystal parts or atomic ordering (Foord and Mills, 1978; Kahr and McBride, 1992; Shtukenberg and Punin, 2007).

Discovery of Cl-rich minerals, such as halite, iowaite, and kuliginite, in the weakly serpentinized Udachnaya East kimberlite is evidence of high chlorine enrichment of the growth medium, but none of these minerals have been described in the Udachnaya-East ultra-fresh low-H_2O kimberlite so far (Fig. 1) (Golovin et al., 2003, 2007; Kamenetsky et al., 2007a, 2008, 2012, 2014). Chlorine and water reach 19.3 wt. % and 12 wt. % in kuliginite and 10.7 wt. % and 26 wt. % in iowaite, respectively.

Experiments simulating serpentinization processes by Rucklidge and Patterson (1977) showed hydroxychloride to be stabilized by alkaline conditions at the reaction front and to be dissolved subsequently as fresh fluids replace those modified by production of serpentine. In another experimental study of Poty et al. (1972), alkaline solutions formed after reaction with olivine in the presence of Cl in an originally acidic environment. Synthesis of oxyhydroxides in chlorinated environments by Rémazeilles and Refait (2007) showed strong influence

This is a preprint, the final version is subject to change, of the American Mineralogist (MSA)
Cite as Authors (Year) Title. American Mineralogist, in press.
DOI: https://doi.org/10.2138/am-2018-6363

of Cl on the formation of akaganeite $(Fe^{3+},Ni^{2+})_8(OH,O)_{16}Cl_{1.25}\cdot nH_2O$.

In our view, the most realistic scenario for the formation of the discussed mineral assemblages in veins and voids, including kuliginite in olivine-rich kimberlitic types, may be as follows. Percolation of external water, possibly Ca-Cl brines from the aquifer system in the host sediments below 510 m, leads to leaching of primary magmatic chlorides, alkali carbonates, and alkali sulfates, as well as to partial serpentinization of rocks. The latter process causes re-distribution of components in the residual saline fluid in veins and voids. Some water is spent on serpentinization of olivine-rich kimberlites, while the residual fluid becomes enriched in Mg and Fe. Kuliginite and iowaite apparently crystallize from this very residual solution enriched in Mg, Fe and Cl. Gypsum and NaCl crystallize simultaneously with kuliginite and iowaite. Finds of fluid inclusions in NaCl provide evidence for hydrothermal origin of NaCl.

According to experimental data Klimchouk (1996), gypsum is unstable above 100 °C even in hydrothermal conditions, and thus the gypsum+kuliginite+iowaite assemblage should crystallize at lower temperatures. The same temperature can be inferred from the composition of iowaite, which shows complete dehydroxylation at 291 °C in heating experiments Frost et al. (2006), while water contents in iowaite of the analyzed samples correspond to a temperature range within 79 °C.

Saini-Eidukat et al. (1994) described hibbingite $Fe_2(OH)_2Cl$ on reinforced steel bars in a swimming pool construction. Other environments where Cl is in contact with Fe-bearing compounds, such as steel in brine, should be checked for the presence of related compounds (Cawthorn et al., 2009). Numerous archaeological studies revealed iron-magnesium hydroxychloride phases on the surface of corroded iron artefacts (Post et al., 2003; Ståhl et al., 2003; Reguer et al., 2007).

Implications

The presence of two non-serpentinized ultra-fresh kimberlite units in the

This is a preprint, the final version is subject to change, of the American Mineralogist (MSA)
Cite as Authors (Year) Title. American Mineralogist, in press.
DOI: https://doi.org/10.2138/am-2018-6363

Udachnaya East kimberlite and available data on melt inclusions in kimberlite minerals offer an exceptional opportunity to study the composition and evolution of kimberlite magma (Golovin et al., 2007; Kamenetsky et al., 2014; Golovin et al., 2017; Kitayama et al., 2017; d′Eyrames et al., 2017; Shatskiy et al., 2017).

Finds of halite in some hydrothermally altered kimberlites lead to confusion about the kimberlite origin. The mineral assemblage in this type of kimberlite, which consists of abundant serpentine around lenses and veins, halite, calcite, iowaite, barite, celestine, gypsum, and kuliginite (Kopylova et al. (2016); this study), has never been reported before for ultra-fresh saline kimberlites (Kamenetsky et al., 2007a, 2008, 2012, 2014). The occurrence intergrowths of kuliginite and iowaite in halite may trace a hydrothermal/metasomatic process of kimberlite alteration by fluids/brines, and metal transport in Cl-bearing solutions. Kuliginite and iowaite intergrowths indicating their simultaneous crystallization at temperatures below 100 °C.

Kuliginite is a new potential constituent of the corrosion system of archaeological iron artefacts buried in soil, on a microscopic scale. Therefore, investigation into Cl-bearing minerals has important implications for preservation of archaeological artefacts and can provide clues to iron corrosion mechanisms.

Acknowledgments

We greatly appreciate the assistance of our colleagues A. V. Vishnevsky (photographs of minerals), E.N. Nigmatulina (EPMA) and I.V. Pekov (optical properties). The study was supported by state assignment project 0330-2016-0006. Comments by T. Alifirova, constructive reviews by Uwe Kolitsch and an anonymous reviewer and the associate editor, G. Diego Gatta, helped to improve many aspects of the paper.

References

Alekseev, S. V. (2009) Permafrost-Groundwater Systems of the Yakutian Diamond Province. Akademicheskoe Izdatelstvo "Geo", Novosibirsk.

Alexeev, S. V., Alexeeva, L. P., Borisov, V. N., Shouakar-Stash, O., Frape, S. K., Chabaux, F., and Kononov, A. M. (2007) Isotopic composition (H, O, Cl, Sr) of ground brines of the Siberian Platform. Russian Geology and Geophysics, 48, 225–236.

Aullon, G., Bellamy, D., Orpen, A. G., Brammer, L., Bruton, F., and Eric, A. (1998) Metal-bound chlorine often accepts hydrogen bonds. Chemical Communications. Royal Society of Chemistry, 6, 653-654.

Braithwaite, R., Mereiter, K., Paar, W., and Clark, A. (2011) Herbertsmithite, $Cu_3Zn(OH)_6Cl_2$, a new species, and the definition of paratacamite. Mineralogical magazine, 68, 527–539.

Braithwaite, R. S. W., Dunn, P. J., Pritchard, R. G., and Parr, W. H. (1994) Iowaite, a re-investigation. Mineralogical Magazine, 58, 77–86.

Brakhfogel, F. F. (1984) Geological aspects of kimberlite magmatism in the northeastern Siberian platform. Siberian Branch of Academy of Sciences of USSSR, 128, 130–135.

Cawthorn, R. G., Luvhimbe, C., and Slabbert, M. (2009) Suspected presence of hibbingite in olivine pyroxenite adjacent to the UG2 chromitite, Bushveld Complex, South Africa. The Canadian Mineralogist, 47, 1075–1085.

Clissold, M. E., Leverett, P., Williams, P. A., Hibbs, D. E., and Nickel, E. H. (2007) The structure of gillardite, the Ni-analogue of herbertsmithite, from Widgiemooltha, Western Australia. The Canadian Mineralogist, 45, 317–320.

Crichton, W. A. and Müller, H. (2017) Centennialite, $CaCu_3(OH)_6Cl_2.nH_2O$, n= 0.7, a new kapellasite-like species, and a reassessment of calumetite. Mineralogical Magazine, 81, 1105–1124.

Davis, G. L., Sobolev, N. V., and Kharkiv, A. D. (1980) New data on the age of Yakutian kimberlites obtained by uranium-lead study of zircons. Doklady Akademii Nauk SSSR, 254, 175–179, (In Russian).

d′Eyrames, E., Thomassot, E., Kitayama, Y., Golovin, A., Korsakov, A., and Ionov, D. (2017) A mantle origin for sulfates in the unusual salty Udachnaya-East kimberlite from sulfur abundances, speciation and their relationship with groundmass carbonates. Bulletin de la Société géologique de France, 188, 1–8.

Drozdov, A. V., Egorov, K. N., Gotovtsev, S. P., and Klimovsky, I. V. (1989) Hydrogeological structure and hydrochemical zonation of the Udachnaya kimberlite pipe. In Combined Permafrost and Hydrogeological Studies, p. 146–155. Institute of Permafrost Siberian Branch of Academy of Sciences, Yakutsk.

Foord, E. E. and Mills, B. A. (1978) Biaxiality in 'isometric' and 'dimetric' crystals. American Mineralogist, 63, 316–325.

Frost, R., Bouzaid, J., Musumeci, A., Kloprogge, J., and Martens, W. (2006) Thermal decomposition of the synthetic hydrotalcite iowaite. Journal of Thermal Analysis and Calorimetry, 86, 437–441.

Frost, R. L., Adebajo, M. O., and Erickson, K. L. (2005) Raman spectroscopy of synthetic and natural iowaite. Spectrochimica Acta Part A: Molecular and Biomolecular Spectroscopy, 61, 613–620.

Golovin, A. V., Sharygin, I. S., and Korsakov, A. V. (2017) Origin of alkaline carbonates in kimberlites of the Siberian craton: Evidence from melt inclusions in mantle olivine of the Udachnaya-East pipe. Chemical Geology, 455, 357–375.

Golovin, A. V., Sharygin, V. V., and Pokhilenko, N. P. (2007) Melt inclusions in olivine phenocrysts in unaltered kimberlites from the Udachnaya-East pipe, Yakutia: Some aspects of kimberlite magma evolution during late crystallization stages. Petrology, 15, 168–183.

Golovin, A. V., Sharygin, V. V., Pokhilenko, N. P., Malkovets, V. G., Kolesov, B. A., and Sobolev, N. V. (2003) Secondary melt inclusions in olivine from unaltered kimberlites of the Udachnaya-East pipe, Yakutia. Doklady Earth Sciences, 388, 93–96.

Hålenius, U., Hatert, F., Pasero, M., and Mills, S. (2016) IMA Commission on New Minerals, Nomenclature and Classification (CNMNC) Newsletter 33. New minerals and nomenclature modifications approved in 2016. Mineralogical Magazine, 80, 1135–1144.

Hamilton, W. C. (1965) Significance tests on the crystallographic R factor. Acta Crystallographica, 18, 502–510.

Hawthorne, F. (1985) Refinement of the crystal structure of botallackite. Mineralogical Magazine, 49, 87–91.

Kahr, B. and McBride, J. M. (1992) Optically anomalous crystals. Angewandte Chemie International Edition, 31, 1–26.

Kamenetsky, M. B., Sobolev, A. V., Kamenetsky, V. S., Maas, R., Danyushevsky, L. V., Thomas, R., Pokhilenko, N. P., and Sobolev, N. V. (2004) Kimberlite melts rich in alkali chlorides and carbonates: a potent metasomatic agent in the mantle. Geology, 32, 845–848.

Kamenetsky, V. S., Golovin, A. V., Maas, R., Giuliani, A., Kamenetsky, M. B., and Weiss, Y. (2014) Towards a new model for kimberlite petrogenesis: Evidence from unaltered kimberlites and mantle minerals. Earth-Science Reviews, 139, 145–167.

Kamenetsky, V. S., Kamenetsky, M. B., Golovin, A. V., Sharygin, V. V., and Maas, R. (2012) Ultrafresh salty kimberlite of the Udachnaya–East pipe (Yakutia, Russia): A petrological oddity or fortuitous discovery? Lithos, 152, 173–186.

Kamenetsky, V. S., Kamenetsky, M. B., Sharygin, V. V., Faure, K., and Golovin, A. V. (2007a) Chloride and carbonate immiscible liquids at the closure of the

kimberlite magma evolution (Udachnaya-East kimberlite, Siberia). Chemical Geology, 237, 384–400.

Kamenetsky, V. S., Kamenetsky, M. B., Sobolev, A. V., Golovin, A. V., Demouchy, S., Faure, K., Sharygin, V. V., and Kuzmin, D. V. (2007b) Olivine in the Udachnaya-East kimberlite (Yakutia, Russia): types, compositions and origins. Journal of Petrology, 49, 823–839.

Kamenetsky, V. S., Kamenetsky, M. B., Sobolev, A. V., Golovin, A. V., Demouchy, S., Faure, K., Sharygin, V. V., and Kuzmin, D. V. (2008) Olivine in the Udachnaya-East kimberlite (Yakutia, Russia): types, compositions and origins. Journal of Petrology, 49, 823–839.

Kamenetsky, V. S., Kamenetsky, M. B., Weiss, Y., Navon, O., Nielsen, T. F., and Mernagh, T. P. (2009) How unique is the Udachnaya-East kimberlite? Comparison with kimberlites from the Slave Craton (Canada) and SW Greenland. Lithos, 112, 334–346.

Kamenetsky, V. S., Sharygin, V. V., Kamenetsky, M. B., and Golovin, A. V. (2006) Chloride-carbonate nodules in kimberlites from the Udachnaya pipe: alternative approach to the evolution of kimberlite magmas. Geochemistry International, 44, 935–940.

Kampf, A. R., Sciberras, M. J., Leverett, P., Williams, P. A., Malcherek, T., Schlüter, J., Welch, M. D., Dini, M., and Donoso, A. M. (2013a) Paratacamite-(Mg), $Cu_3(Mg, Cu)Cl_2(OH)_6$; a new substituted basic copper chloride mineral from Camerones, Chile. Mineralogical Magazine, 77, 3113–3124.

Kampf, A. R., Sciberras, M. J., Williams, P. A., Dini, M., and Donoso, A. (2013b) Leverettite from the Torrecillas mine, Iquique Provence, Chile: the Co-analogue of herbertsmithite. Mineralogical Magazine, 77, 3047–3054.

Kharkiv, A. D., Zinchuk, N. N., and Kryuchkov, A. I. (1998) Primary diamond deposits of the world, 555 p. Nedra, Moscow.

Kinny, P. D., Griffin, B. J., Heaman, L. M., Brakhfogel, F. F., and Spetsius, Z. V. (1997) SHRIMP U-Pb ages of perovskite from Yakutian kimberlites. Russian Geology and Geophysics, 38, 97–105.

Kitayama, Y., Thomassot, E., Galy, A., Golovin, A., Korsakov, A., d'Eyrames, E., Assayag, N., Bouden, N., and Ionov, D. (2017) Co-magmatic sulfides and sulfates in the Udachnaya-East pipe (Siberia): A record of the redox state and isotopic composition of sulfur in kimberlites and their mantle sources. Chemical Geology, 455, 315–330.

Klimchouk, A. (1996) The dissolution and conversion of gypsum and anhydrite. International Journal of Speleology, 25, 2–16.

Kopylova, M. G., Gaudet, M., Kostrovitsky, S. I., Polozov, A. G., and Yakovlev, D. A. (2016) Origin of salts and alkali carbonates in the Udachnaya East kimberlite: Insights from petrography of kimberlite phases and their carbonate and evaporite xenoliths. Journal of Volcanology and Geothermal Research, 327, 116–134.

Kozlov, I. and Levshov, P. (1962) Amakinite, a new mineral of the brucite-pyrochroite group. American Mineralogist, 47, 1218.

Krause, W., Bernhardt, H.-J., Braithwaite, R. S. W., Kolitsch, U., and Pritchard, R. (2006) Kapellasite, $Cu_3Zn(OH)_6Cl_2$, a new mineral from Lavrion, Greece, and its crystal structure. Mineralogical Magazine, 70, 329–340.

Libowitzky, E. (1999) Correlation of OH stretching frequencies and OH$\cdots$O hydrogen bond lengths in minerals. Monatshefte fur Chemie, 130, 1047-1059.

Maas, R., Kamenetsky, M. B., Sobolev, A. V., Kamenetsky, V. S., and Sobolev, N. V. (2005) Sr, Nd, and Pb isotope evidence for a mantle origin of alkali chlorides and carbonates in the Udachnaya kimberlite, Siberia. Geology, 33, 549–552.

Malcherek, T., Bindi, L., Dini, M., Ghiara, M., Donoso, A. M., Nestola, F., Rossi, M., and Schlüter, J. (2014) Tondiite, $Cu_3Mg(OH)_6Cl_2$, the Mg-analogue of herbertsmithite. Mineralogical Magazine, 78, 583–590.

Malcherek, T. and Schlüter, J. (2009) Structures of the pseudo-trigonal polymorphs of $Cu_2(OH)_3Cl$. Acta Crystallographica Section B: Structural Science, 65, 334–341.

Marshintsev, V. K., Migalkin, K. N., Nikolaev, N. S., and Barashkov, I. P. (1976) Unchanged kimberlite of Udachnaya-Vostochnaya pipe. Doklady Akademii Nauk SSSR, 231, 961–964.

Mascal, M. (1997) A statistical analysis of halide H–A (A= OR, NR 2, N+ R 3) hydrogen bonding interactions in the solid state. Journal of the Chemical Society, Perkin Transactions 2, 10, 1999–2001.

Mernagh, T. P., Kamenetsky, V. S., and Kamenetsky, M. B. (2011) A Raman microprobe study of melt inclusions in kimberlites from Siberia, Canada, SW Greenland and South Africa. Spectrochimica Acta Part A: Molecular and Biomolecular Spectroscopy, 80, 82–87.

Momma, K. and Izumi, F. (2011) VESTA 3 for three-dimensional visualization of crystal, volumetric and morphology data. Journal of Applied Crystallography, 44, 1272–1276.

Nishio-Hamane, D., Momma, K., Ohnishi, M., Shimobayashi, N., Miyawaki, R., Tomita, N., Okuma, R., Kampf, A., and Minakawa, T. (2017) Iyoite, $MnCuCl(OH)_3$ and misakiite, $Cu_3Mn(OH)_6Cl_2$: new members of the atacamite family from Sadamisaki Peninsula, Ehime Prefecture, Japan. Mineralogical Magazine, 81, 485–498.

Palatinus, L. and Chapuis, G. (2007) SUPERFLIP – a computer program for the solution of crystal structures by charge flipping in arbitrary dimensions. Journal of Applied Crystallography, 40, 786–790.

514 Parise, J. B. and Hyde, B. G. (1986) The structure of atacamite and its re-
515 lationship to spinel. Acta Crystallographica Section C: Crystal Structure
516 Communications, 42, 1277–1280.

517 Petrícek, V., Dusek, M., and Palatinus, L. (2014) Crystallographic computing
518 system JANA2006: general features. Zeitschrift für Kristallographie. Crys-
519 talline materials, 229, 345–352.

520 Post, J. E., Heaney, P. J., Dreele, R. B. V., and Hanson, J. C. (2003) Neu-
521 tron and temperature-resolved synchrotron X-ray powder diffraction study of
522 akaganéite. American Mineralogist, 88, 782–788.

523 Poty, B., Holland, H. D., and Borcsik, M. (1972) Solution-mineral equilibria
524 in the system MgO-SiO_2-H_2O-$MgCl_2$ at 500 °C and 1 kbar. Geochimica et
525 Cosmochimica Acta, 36, 1101–1113.

526 Reguer, S., Neff, D., Bellot-Gurlet, L., and Dillmann, P. (2007) Deterioration
527 of iron archaeological artefacts: micro-Raman investigation on Cl-containing
528 corrosion products. Journal of Raman Spectroscopy, 38, 389–397.

529 Rémazeilles, C. and Refait, P. (2007) On the formation of β-FeOOH (akaganéite)
530 in chloride-containing environments. Corrosion Science, 49, 844–857.

531 Rogers, A. F. (1924) Kempite, a new manganese mineral from California. Amer-
532 ican Journal of Science, 44, 145–150.

533 Rucklidge, J. C. and Patterson, G. C. (1977) The role of chlorine in serpen-
534 tinization. Contributions to Mineralogy and Petrology, 65, 39–44.

535 Saini-Eidukat, B., Kucha, H., and Keppler, H. (1994) Hibbingite, $Fe_2(OH)_3Cl$, a
536 new mineral from the Duluth Complex, Minnesota, with implications for the
537 oxidation of Fe-bearing compounds and the transport of metals. American
538 Mineralogist, 79, 555–561.

539 Sciberras, M. J., Leverett, P., Williams, P. A., Hibbs, D. E., Downes,
540 P. J., Welch, M. D., and Kampf, A. R. (2013) Paratacamite-(Ni),

$Cu_3(Ni,Cu)Cl_2(OH)_6$, a new mineral from the Carr Boyd Rocks mine, Western Australia. Australian Journal of Mineralogy, 17, 39–44.

Shatskiy, A., Litasov, K. D., Sharygin, I. S., and Ohtani, E. (2017) Composition of primary kimberlite melt in a garnet lherzolite mantle source: constraints from melting phase relations in anhydrous Udachnaya-East kimberlite with variable CO_2 content at 6.5 GPa. Gondwana Research, 45, 208–227.

Shtukenberg, A. and Punin, Y. O. (2007) Stress induced optical anomalies. In A. Shtukenberg, Shtukenberg Y and Kahr, Eds., Optically anomalous crystal, 35-94 p. Springer. Dordrecht.

Smith, B. H. S., Nowicki, T. E., Russell, J. K., Webb, K. J., Mitchell, R. H., Hetman, C. M., Harder, M., Skinner, E., and Robey, J. A. (2013) Kimberlite terminology and classification, Eds., Proceedings of 10^{th} International Kimberlite Conference, p. 1-17. Springer. New Delhi.

Ståhl, K., Nielsen, K., Jiang, J., Lebech, B., Hanson, J. C., Norby, P., and van Lanschot, J. (2003) On the akaganéite crystal structure, phase transformations and possible role in post-excavational corrosion of iron artifacts. Corrosion Science, 45, 2563–2575.

Steiner, T. (1998) Hydrogen-bond distances to halide ions in organic and organometallic crystal structures: up-to-date database study. Acta Crystallographica Section B: Structural Science, 54, 456–463.

Toby, B. H. and Von Dreele, R. B. (2013) GSAS-II: the genesis of a modern open-source all purpose crystallography software package. Journal of Applied Crystallography, 46, 544–549.

Welch, M. D., Sciberras, M. J., Williams, P. A., Leverett, P., Schlüter, J., and Malcherek, T. (2014) A temperature-induced reversible transformation between paratacamite and herbertsmithite. Physics and Chemistry of Minerals, 41, 33–48.

Yudin, D. S., Tomilenko, A. A., Alifirova, T. A., Travin, A. V., Murzintsev, N. G., and Pokhilenko, N. P. (2011) Results of $^{40}Ar/^{39}Ar$ dating of phlogopites from kelyphitic rims around garnet grains (Udachnaya-Vostochnaya kimberlite pipe). Doklady Earth Sciences, 469, 728–731.

List of Figures

This is a preprint, the final version is subject to change, of the American Mineralogist (MSA)
Cite as Authors (Year) Title. American Mineralogist, in press.
DOI: https://doi.org/10.2138/am-2018-6363

617 # Figures

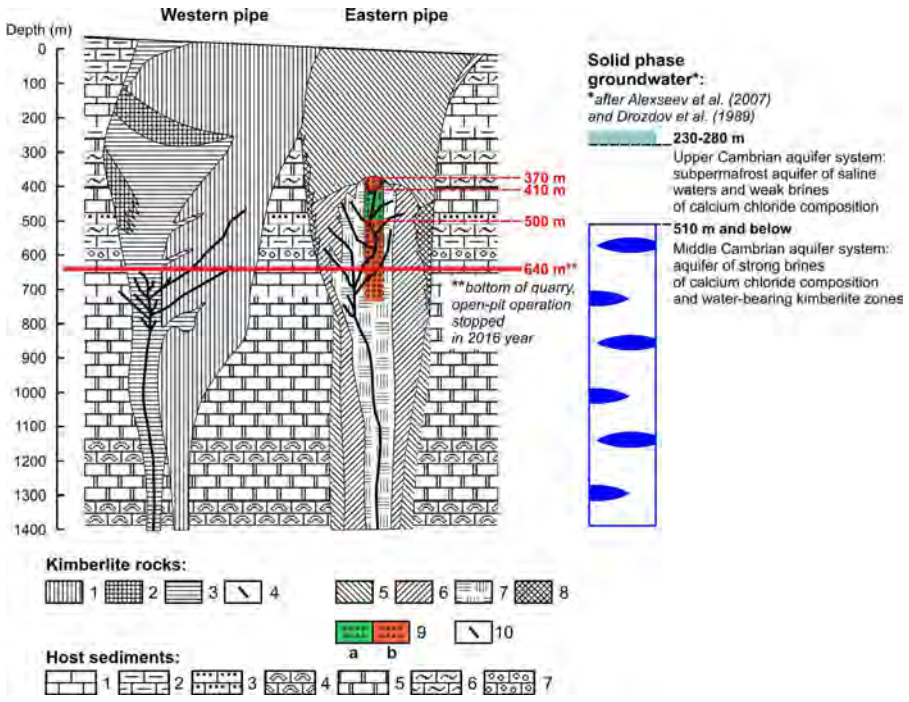

Figure 1: Geological section of the Udachnaya kimberlite pipe according to Kryuchkov and Sviridov (modified by Golovin et al. (2017) after Fig. 47 from Kharkiv et al. (1998)). 1-4 = western body with volcaniclastic kimberlite (1-3; separated units, which have well defined boundaries) and veins of coherent kimberlite (4). 5-10 = eastern body consisting of volcaniclastic kimberlite (5-9, separated units), and veins of coherent kimberlites (10). Volcaniclastic kimberlite (9): (a) Green = unserpentinized fresh kimberlites (for details see Kamenetsky et al. (2012, 2014)), the 410-500 m depth interval; (b) Rusty = partially serpentinized kimberlites at 370-410 m and 500-640 m. The upper boundary for kimberlites (9) at 370 m is according to Kharkiv et al. (1998) and Marshintsev et al. (1976); other boundaries were constrained during 2003-2016 field work in the quarry. Host sediments (after Alekseev (2009)): limestones (1 - clear, 2 - silty, 3 - sandy, 4 - organogenic), dolomites (5), marls (6), calcareous conglomerates (7).

This is a preprint, the final version is subject to change, of the American Mineralogist (MSA)
Cite as Authors (Year) Title. American Mineralogist, in press.
DOI: https://doi.org/10.2138/am-2018-6363

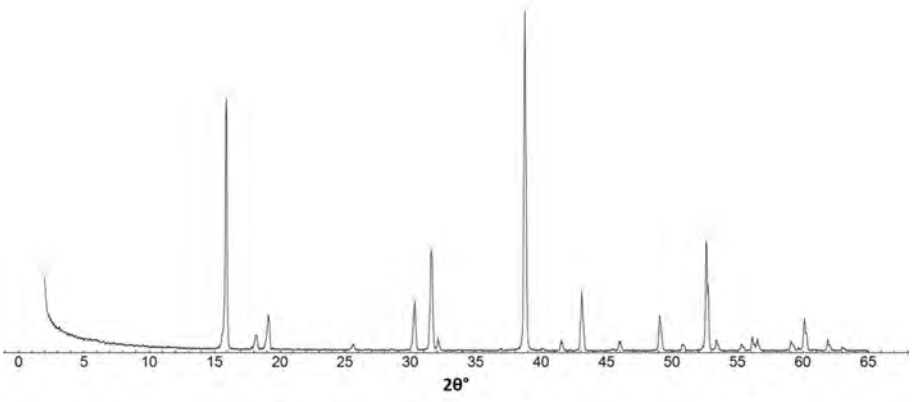

Figure 2: Powder X-ray diffraction pattern of kuliginite (Cu $K\alpha$ radiation).

This is a preprint, the final version is subject to change, of the American Mineralogist (MSA)
Cite as Authors (Year) Title. American Mineralogist, in press.
DOI: https://doi.org/10.2138/am-2018-6363

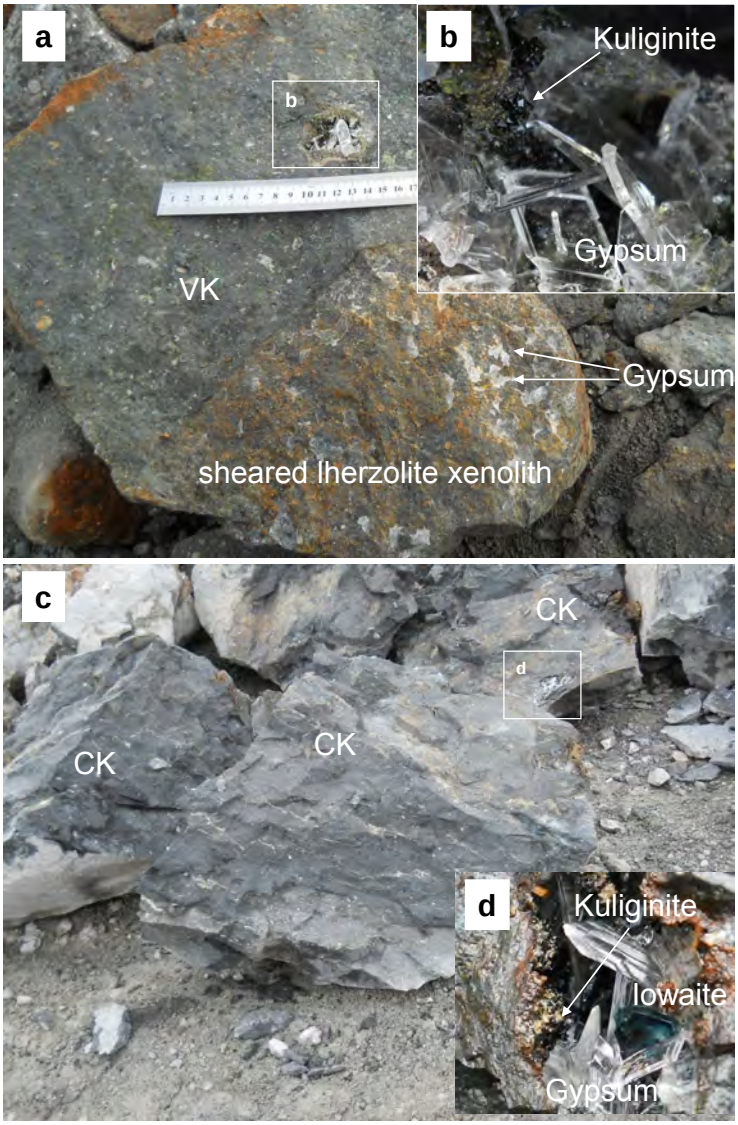

Figure 3: (a) Volcaniclastic (VK) and (c) coherent (CK) kimberlites from Udachnaya-East pipe. VK and CK corresponds to unit 9b and 10, respectively from Fig. 1. (b) kuliginite with gypsum in void from VK. (d) paragenesis of kuliginite, iowaite and gypsum in lens from CK.

This is a preprint, the final version is subject to change, of the American Mineralogist (MSA)
Cite as Authors (Year) Title. American Mineralogist, in press.
DOI: https://doi.org/10.2138/am-2018-6363

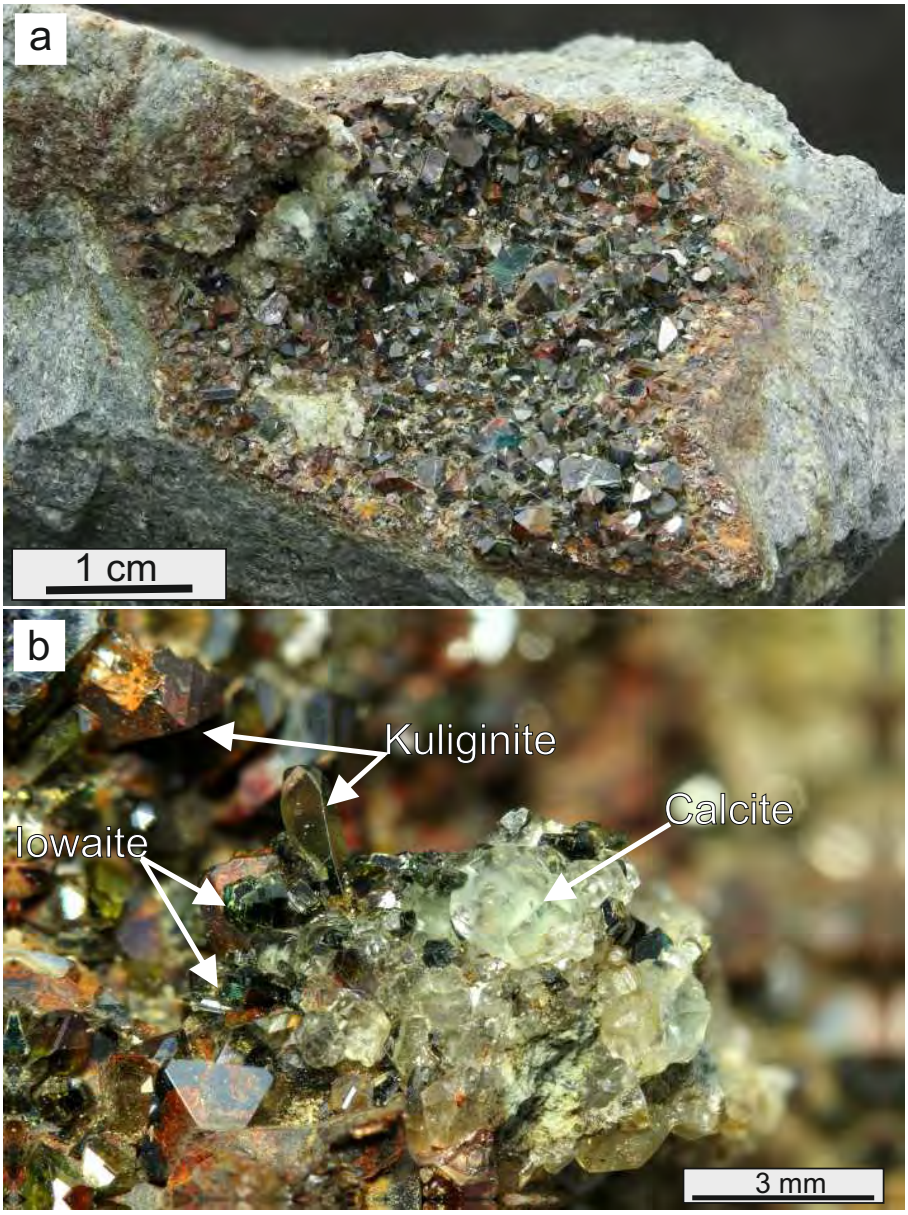

Figure 4: (a): Geode of kuliginite, iowaite and calcite in the Udachnaya East kimberlite pipe; (b): Photo of green transparent kuliginite crystals coexisting with dark green iowaite and white calcite crystals.

This is a preprint, the final version is subject to change, of the American Mineralogist (MSA)
Cite as Authors (Year) Title. American Mineralogist, in press.
DOI: https://doi.org/10.2138/am-2018-6363

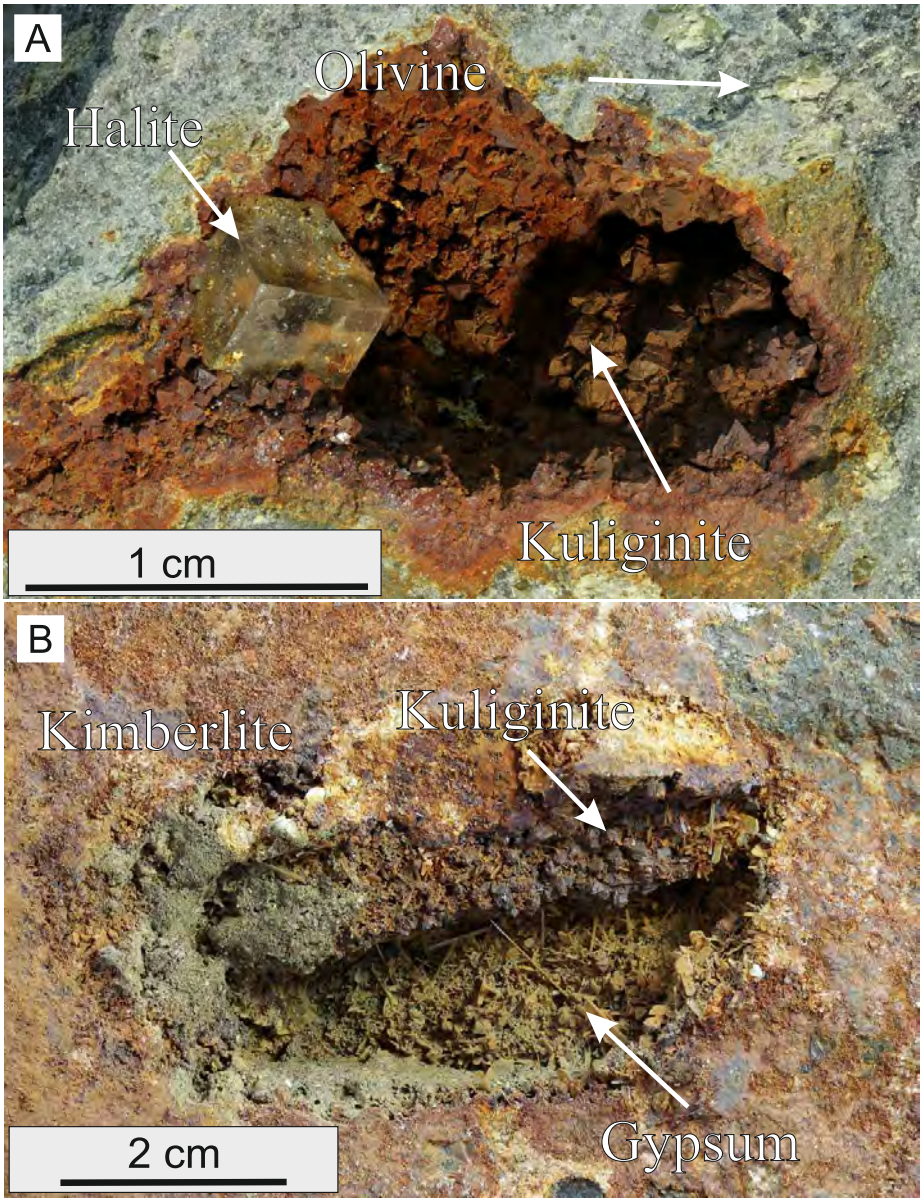

Figure 5: (a): Geode with a colorless halite and kuliginite crystal; (b): Photograph of geode with gypsum and kuliginite in kimberlite.

This is a preprint, the final version is subject to change, of the American Mineralogist (MSA)
Cite as Authors (Year) Title. American Mineralogist, in press.
DOI: https://doi.org/10.2138/am-2018-6363

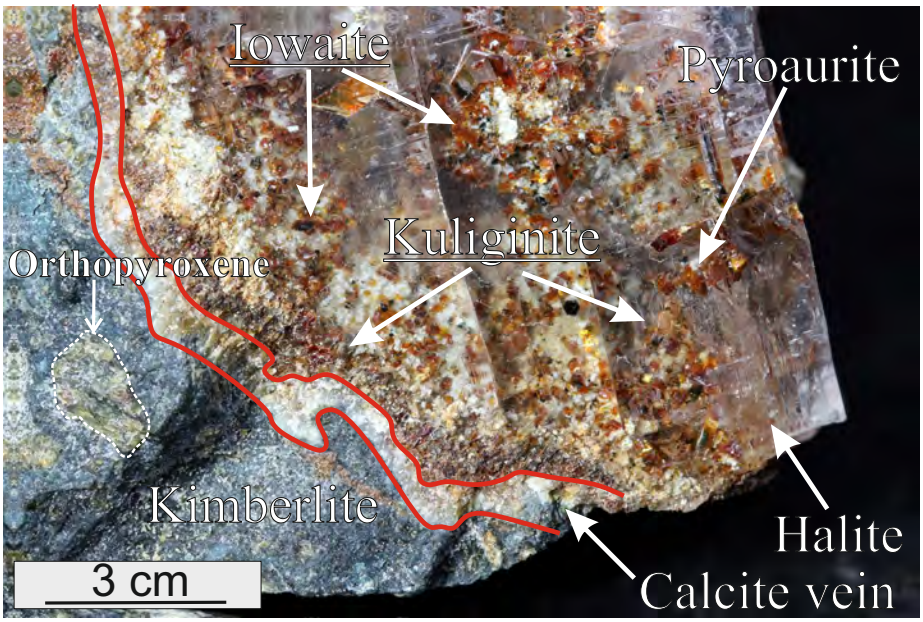

Figure 6: Contact of kimberlite and halite nodules with red rust iowaite.

This is a preprint, the final version is subject to change, of the American Mineralogist (MSA)
Cite as Authors (Year) Title. American Mineralogist, in press.
DOI: https://doi.org/10.2138/am-2018-6363

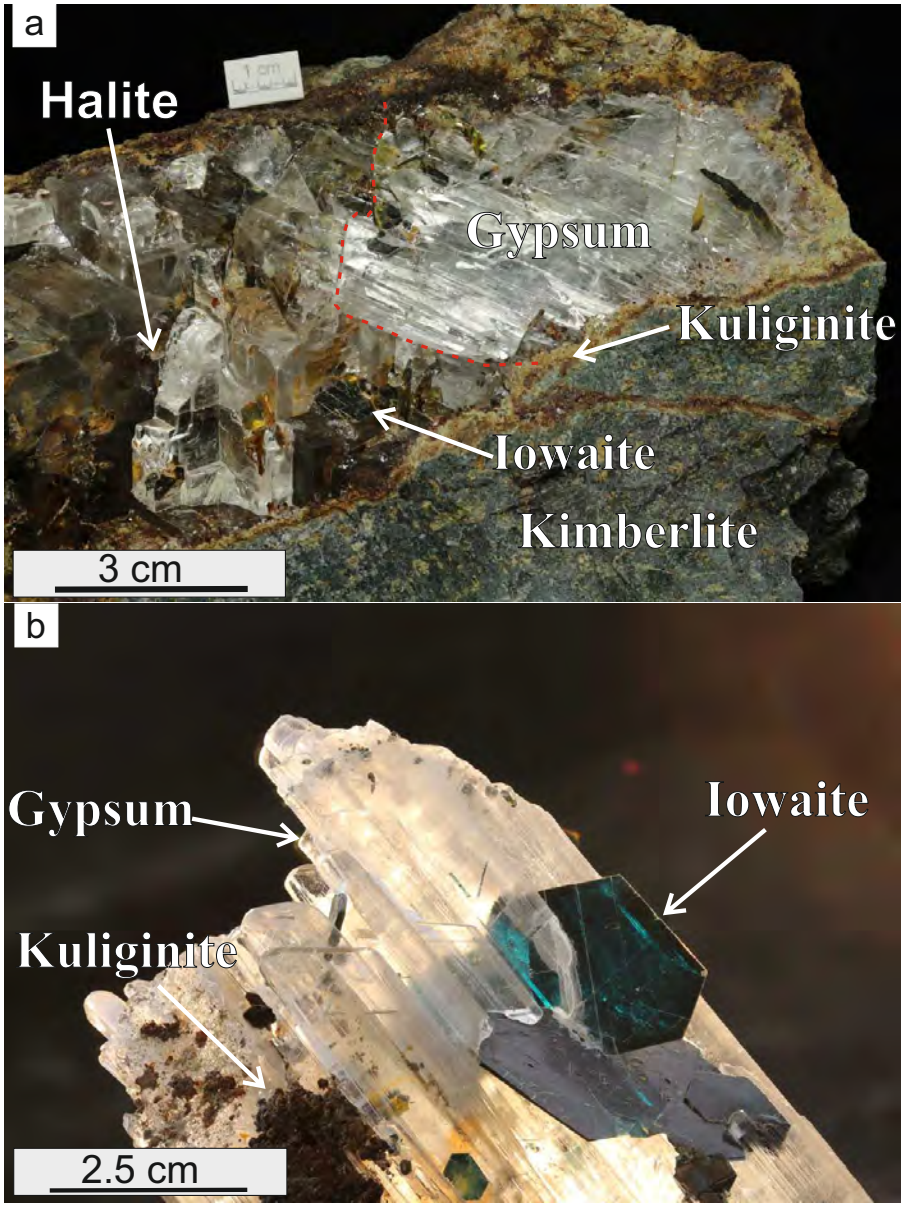

Figure 7: (a): Gypsum and iowaite crystals in halite from the Udachnaya East kimberlite pipe; (b): Photo of gypsum and iowaite crystal.

This is a preprint, the final version is subject to change, of the American Mineralogist (MSA)
Cite as Authors (Year) Title. American Mineralogist, in press.
DOI: https://doi.org/10.2138/am-2018-6363

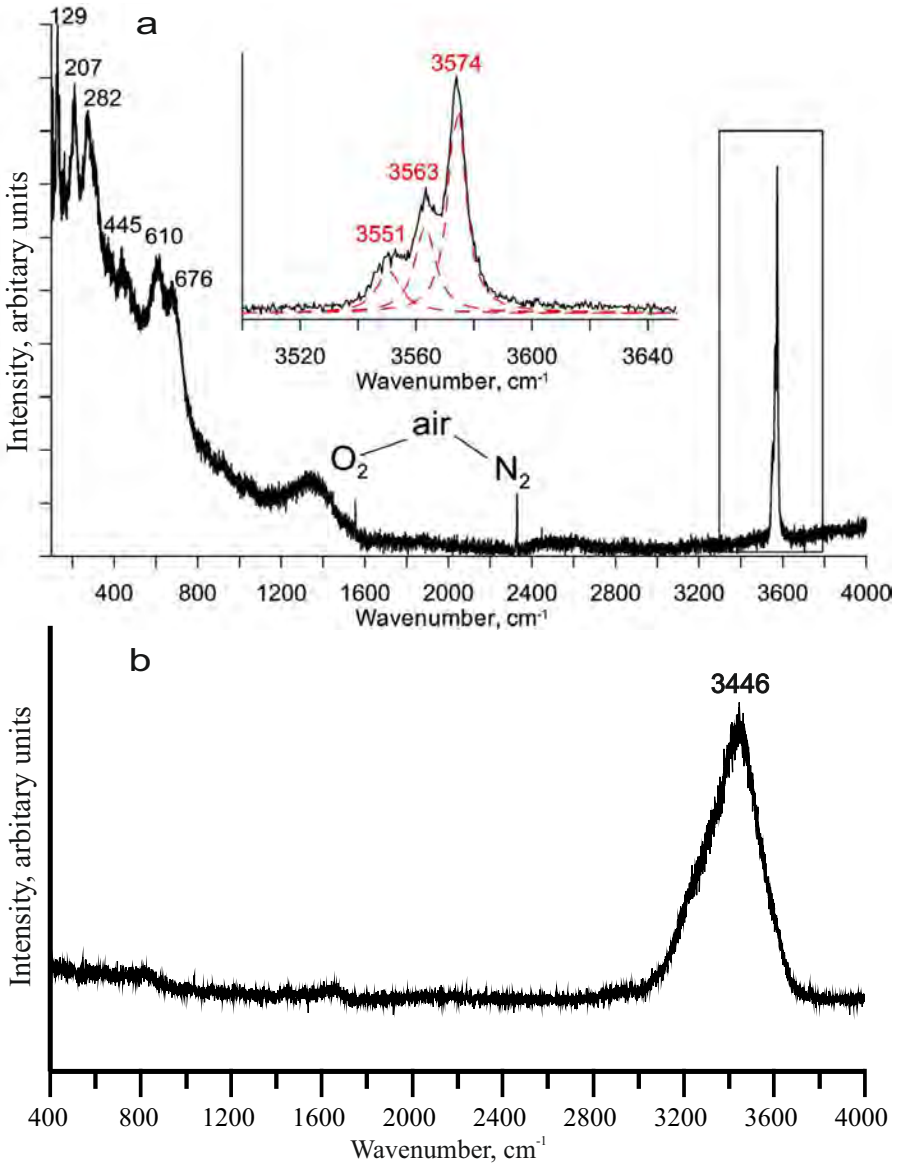

Figure 8: (a): Raman spectrum of kuliginite. See Table 7 for assignment of Raman bands; (b): Raman spectra of a H_2O inclusion in halite.

This is a preprint, the final version is subject to change, of the American Mineralogist (MSA)
Cite as Authors (Year) Title. American Mineralogist, in press.
DOI: https://doi.org/10.2138/am-2018-6363

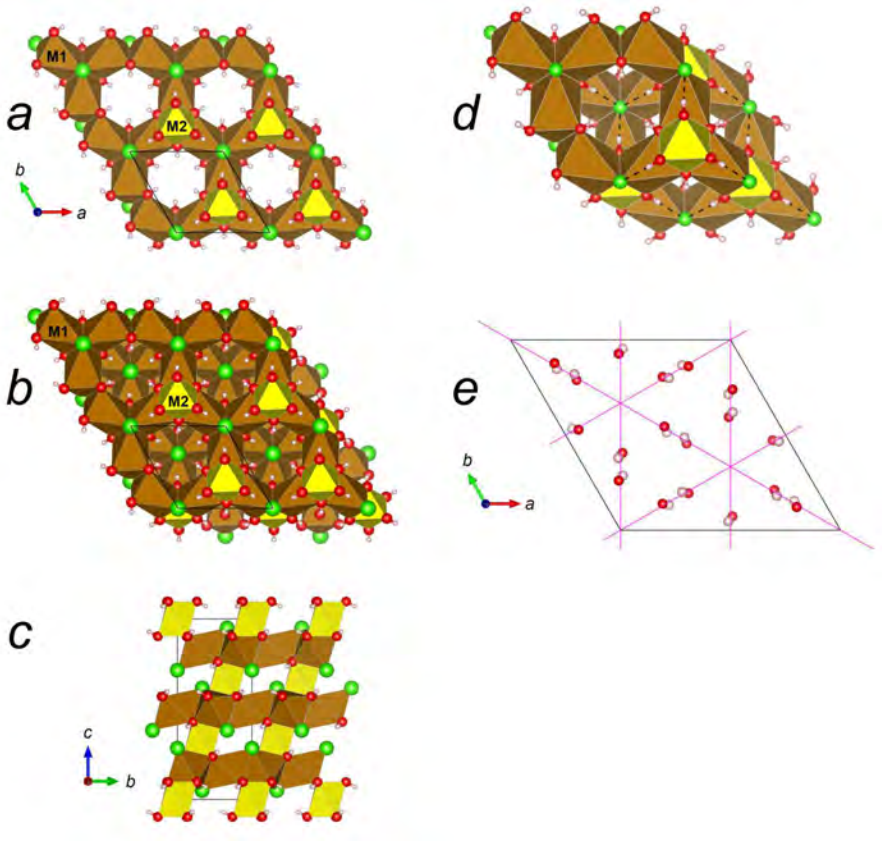

Figure 9: Crystal structure of kuliginite: (a) - single gibbsite-type layers of $Fe(OH)_4Cl_2$ octahedra with $(Mg,Fe)(OH)_6$ octahedra on the triple junctions; (b-c) - stacking of gibbsite-type layers via $(Mg,Fe)(OH)_6$ octahedra; (d) - arrangement of O-H$\cdots$Cl hydrogen bonds (dashed lines); (e) - displacement of oxygen and hydrogen atoms from possible {110} mirror planes. M1- and M2-centered octahedra are given in brown and yellow, respectively. Cl, O, and H are given in green, red, and pink, respectively. The figure was prepared using VESTA software (Momma and Izumi, 2011).

This is a preprint, the final version is subject to change, of the American Mineralogist (MSA)
Cite as Authors (Year) Title. American Mineralogist, in press.
DOI: https://doi.org/10.2138/am-2018-6363

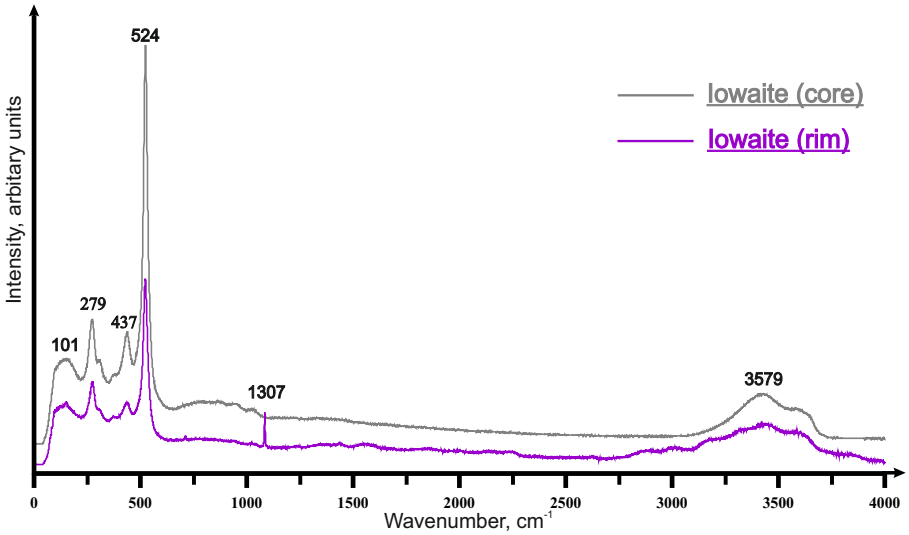

Figure 10: Raman spectra of iowaite.

This is a preprint, the final version is subject to change, of the American Mineralogist (MSA)
Cite as Authors (Year) Title. American Mineralogist, in press.
DOI: https://doi.org/10.2138/am-2018-6363

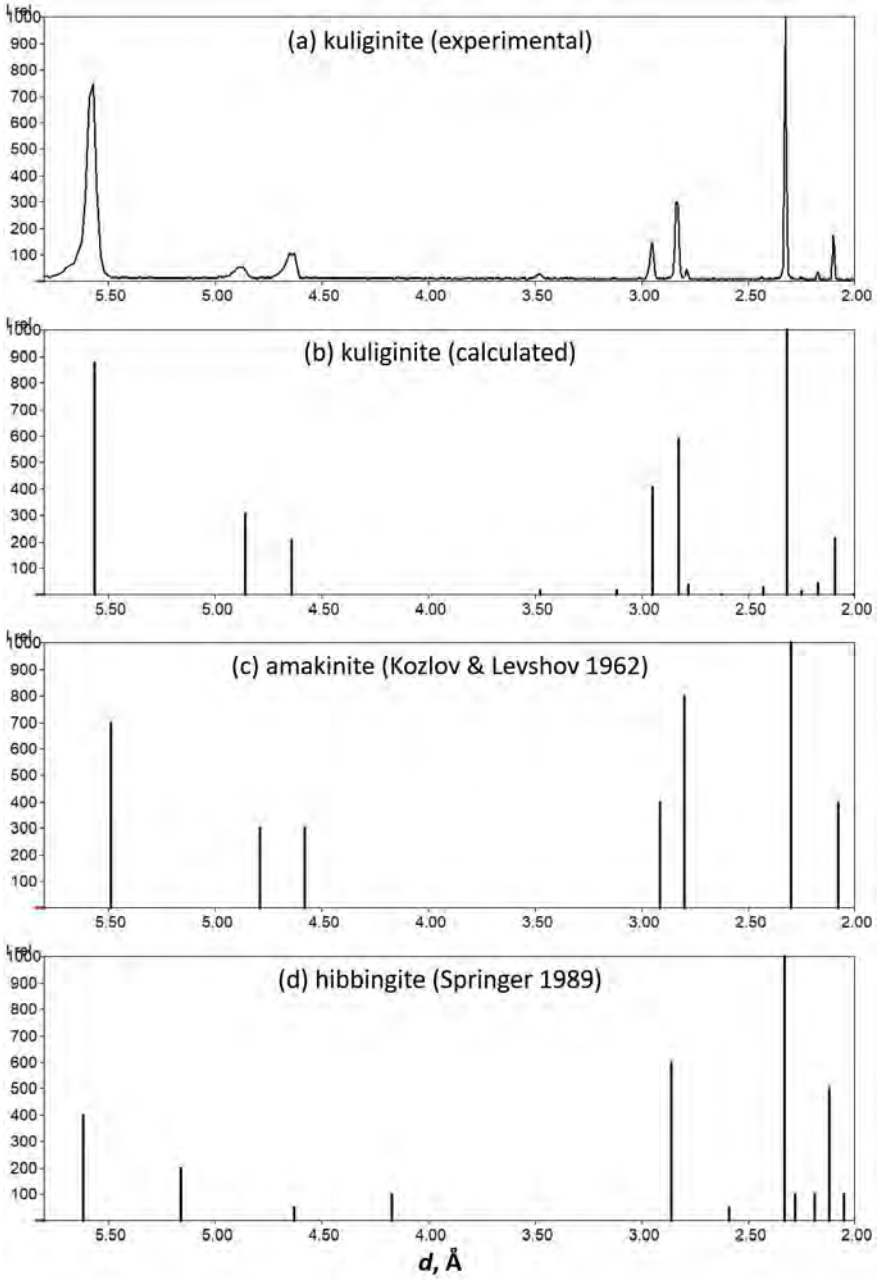

Figure 11: X-ray diffraction of kuliginite-related minerals.

This is a preprint, the final version is subject to change, of the American Mineralogist (MSA)
Cite as Authors (Year) Title. American Mineralogist, in press.
DOI: https://doi.org/10.2138/am-2018-6363

Table 1. Chemical composition (wt. %) of different minerals occurring together with kuliginite from Udachnaya kimberlite pipe (C–center; R–rim).

	Kuliginite C	Detection limits	avg (n=40)	std (n=40)	Iowaite C	Iowaite R	Celestine C
SiO_2	0.00	0.052	0.02	0.02	b.d.	0.36	b.d.
Al_2O_3	0.01	0.015	0.01	0.02	0.6	0.51	b.d.
FeO	57.7	0.013	57.3	0.26	24.5	24.7	b.d.
MnO	2.26	0.012	2.14	0.13	b.d.	b.d	b.d.
MgO	9.79	0.018	9.68	0.39	36.8	34.3	b.d.
CaO	0.02	0.007	0.01	0.01	b.d.	0.69	b.d.
Na_2O	0.01	0.013	0.02	0.02	0.23	0.63	b.d.
K_2O	0.00	0.006	0.00	0.01	b.d.	0.12	b.d.
Cl	19.3	0.016	19.3	0.24	10.7	9	b.d.
F	0.11	0.015	0.15	0.03	b.d.	b.d.	b.d.
P_2O_5	0.03	0.020	0.02	0.02	b.d.	b.d.	b.d.
SrO	b.d.	0.011	–	–	b.d.	b.d.	44.1
BaO	0.02	0.018	0.01	0.01	b.d.	b.d.	12.7
SO_3	0.00	0.008	0.01	0.01	b.d.	b.d.	43.3
H_2O*	11.6	–	–	–	–	–	–
Total	100.8	–	–	–	72.8	70.2	100.0

b.d. – below detection limit; dash- not analysed

H_2O* - calculated from structural data

This is a preprint, the final version is subject to change, of the American Mineralogist (MSA)
Cite as Authors (Year) Title. American Mineralogist, in press.
DOI: https://doi.org/10.2138/am-2018-6363

Table 2. Bond lengths for M1 and M2 sites in kuliginite structure and corresponding bond-valence sums (BVSs) for different cations (Brese and O'Keeffe 1991)

M1−O1	2.0477(9)	M2−O1	2.1029(11)
M1−O1	2.0477(9)	M2−O1	2.1029(12)
M1−O1	2.1466(14)	M2−O1	2.1029(12)
M1−O1	2.1466(14)	M2−O1	2.1029(11)
M1−Cl1	2.6363(5)	M2−O1	2.1029(12)
M1−Cl1	2.6363(5)	M2−O1	2.1029(12)
bvs for Fe^{2+}	**1.93**		2.21
bvs for Mg^{2+}	1.8		**1.98**
bvs for Mn^{2+}	2.27		2.58

This is a preprint, the final version is subject to change, of the American Mineralogist (MSA)
Cite as Authors (Year) Title. American Mineralogist, in press.
DOI: https://doi.org/10.2138/am-2018-6363

Table 3. Crystal data, data collection and structure refinement details.

Chemical formula	$Cl_2Fe_{2.98}H_6Mg_{0.91}Mn_{0.11}O_6$
M_r	367.5
Crystal system, space group	Trigonal, $R\bar{3}$
a, c (Å)	6.9521(5), 14.5740(11)
V (Å^3)	610.02(8)
Z	3
Density (g/cm^3)	3.001
Absorption coefficient	6.11 mm^{-1}
F_{000}	536
Radiation type	Mo $K\alpha$
Crystal size (mm)	0.56 × 0.37 × 0.08
θ range	3.6–31.7°
hkl range	$-10 \le h \le 10$; $-10 \le k \le 10$; $-20 \le l \le 21$
No. of measured, independent and observed [I > 3σ(I)] reflections	3701, 464, 446
R_{int}	0.04
R, wR, S for observed reflections	0.017, 0.048, 1.65
R, wR, S for all reflections	0.018, 0.048, 1.62
No. of parameters	28
$\Delta\rho_{max}$, $\Delta\rho_{min}$ (e Å^{-3})	0.50, -0.40

This is a preprint, the final version is subject to change, of the American Mineralogist (MSA)
Cite as Authors (Year) Title. American Mineralogist, in press.
DOI: https://doi.org/10.2138/am-2018-6363

Table 4. Fractional atomic coordinates and isotropic or equivalent isotropic displacement parameters (Å^2)

site	*Wyckoff*	*x*	*y*	*z*	U_{iso}*/U_{eq}	*occupancy*
M1	9e	0.5	0	0	0.01064(14)	$Fe_{0.965(5)}Mg_{0.035(5)}$
M2	3b	0.333333	−0.333333	0.166667	0.0091(3)	$Mg_{0.853(5)}Fe_{0.147(5)}$
O1	18f	0.21174(15)	−0.19457(14)	0.07057(7)	0.0124(4)	O
H1	18f	0.148(3)	−0.130(3)	0.0987(16)	0.023(5)*	H
Cl1	6c	0.666667	0.333333	0.11729(4)	0.01374(17)	Cl

This is a preprint, the final version is subject to change, of the American Mineralogist (MSA)
Cite as Authors (Year) Title. American Mineralogist, in press.
DOI: https://doi.org/10.2138/am-2018-6363

Table 5. Powder X-ray diffraction pattern of kuliginite. Measured values obtained from Pawley refinement using GSAS-II software (Toby and Von Dreele, 2013) are compared with those calculated from structural model.

h	*k*	*l*	d_{meas} (Å)	I_{meas}	d_{calc} (Å)	I_{calc}
1	0	1	5.566	667	5.565	964
0	0	3	4.87	58	4.858	309
1	0	-2	4.645	130	4.641	236
1	1	0	3.475	23	3.476	26
1	0	4	3.123	3	3.117	12
2	0	-1	2.948	157	2.948	406
1	1	3	2.829	177	2.827	286
1	1	-3	2.829	177	2.827	350
2	0	2	2.783	29	2.782	35
1	0	-5	2.629	1	2.624	5
0	0	6	2.435	5	2.429	26
2	0	-4	2.323	1000	2.321	1000
3	-1	1	2.248	4	2.248	3
2	1	1	2.248	4	2.248	9
2	1	-2	2.172	15	2.172	28
3	-1	-2	2.172	15	2.172	18
2	0	5	2.096	195	2.094	203
3	0	0	2.006	1	2.007	0
1	1	-6	1.994	3	1.991	5
1	1	6	1.994	3	1.991	4
1	0	7	1.972	36	1.968	123
3	-1	4	1.931	1	1.93	1
2	1	4	1.931	1	1.93	1
3	0	-3	1.855	65	1.855	176
3	0	3	1.855	65	1.855	24
3	-1	-5	1.795	14	1.794	14
2	1	-5	1.795	14	1.794	10
1	0	-8	1.748	4	1.744	7
2	2	0	1.738	370	1.738	331
2	0	-7	1.715	34	1.712	33
4	-1	-1	1.659	12	1.659	19
3	1	-1	1.659	12	1.659	27
2	2	-3	1.637	22	1.636	32
2	2	3	1.637	22	1.636	26
4	-1	2	1.628	17	1.628	31
3	1	2	1.628	17	1.628	27
0	0	9	1.623	3	1.619	19
2	0	8	1.561	38	1.559	136
3	0	6	1.548	2	1.547	2
3	0	-6	1.548	2	1.547	4
3	-1	7	1.538	62	1.536	94
2	1	7	1.538	62	1.536	81
3	1	-4	1.518	1	1.518	1
4	-1	-4	1.518	1	1.518	3
4	0	1	1.497	37	1.497	51
4	0	-2	1.474	13	1.474	22

This is a preprint, the final version is subject to change, of the American Mineralogist (MSA)
Cite as Authors (Year) Title. American Mineralogist, in press.
DOI: https://doi.org/10.2138/am-2018-6363

1	1	-9	1.471	0	1.468	0
1	1	9	1.471	0	1.468	1
4	-1	5	1.45	2	1.449	1
3	1	5	1.45	2	1.449	0

This is a preprint, the final version is subject to change, of the American Mineralogist (MSA)
Cite as Authors (Year) Title. American Mineralogist, in press.
DOI: https://doi.org/10.2138/am-2018-6363

Table 6. Comparison of Raman peaks of kuliginite with those of $Fe_2(OH)_3Cl$ and their assignment according to Reguer et al., (2007)

Raman bands of kuliginite	$Fe_2(OH)_3Cl$ (Reguer et al. 2007)	Suggested assigment
129	127	–
–	160	O-Fe-O bending mode
207	200	–
282	–	–
–	318	Fe-Cl stretching vibration
445	423	Fe-O stretching vibration
610	618	–
676	–	Mg-O stretching vibration
–	804	Hydroxyl deformation mode
3551	3552	Hydroxyl stretching vibration

This is a preprint, the final version is subject to change, of the American Mineralogist (MSA)
Cite as Authors (Year) Title. American Mineralogist, in press.
DOI: https://doi.org/10.2138/am-2018-6363

Table 7. Mineral species of atacamite group (note that cation sites are separated in the formulae)

	Brucite-like stacking	Spinel-like stacking
Monoclinic	botallackite (Hawthorne, 1985) $CuCu(OH)_3Cl$, $P2_1/m$ a = 5.717(1), b = 6.126(1), c = 5.636(1) Å β = 93.07(1)°	clinoatacamite (Malcherek and Schlüter, 2009) $Cu_2CuCu(OH)_6Cl_2$, $P2_1/n$ a = 6.1226(3), b = 6.8346(4), c = 9.1841(6) β = 99.577(4)
	iyoite (Nishio–Hamane et al., 2017) $CuMn(OH)_3Cl$, $P2_1/m$ a = 5.717(2), b = 6.586(2), c = 5.623(3) Å β = 88.45(3)° (91.55(3)° in conventional setting)	
Orthorhombic		atacamite (Parise and Hyde, 1986) $CuCu(OH)_3Cl$, Pnma a = 6.030 (2) b = 6.865 (2), c = 9.120 (2) Å
		kempite (Rogers, 1924) $[MnMn(OH)_3Cl]$* a = 6.49, b = 7.12, c = 9.52 Å
		hibbingite (Saini-Eidukat et al., 1994) $[FeFe(OH)_3Cl]$* a = 6.31(6), c = 7.10(7), b = 9.20(4) Å
Trigonal	kapellasite (Krause et al., 2006) $Cu_3Zn(OH)_6Cl_2$, P–3m1 a = 6.300(1), c = 5.733(1) Å	herbertsmithite (Braithwaite et al., 2004) $Cu_3Zn(OH)_6Cl_2$, R–3m a = 6.834(1), c = 14.075(2) Å
	haydeeite (Malcherek and Schlüter, 2007) $Cu_3Mg(OH)_6Cl_2$, P–3m1 a = 6.2733(4), c = 5.7472(5) Å	gillardite (Clissold et al., 2007) $Cu_3Ni(OH)_6Cl_2$, R–3m a = 6.8364(1), c = 13.8459(4) Å
	misakiite (Nishio–Hamane et al., 2017) $Cu_3Mn(OH)_6Cl_2$, P–3m1 a = 6.4156(4), c = 5.7026(5) Å	leverettite (Kampf et al., 2013a) $Cu_3Co(OH)_6Cl_2$, R–3m a = 6.8436(6), c = 14.064(1) Å
	centennialite (Crichton and Müller, 2017) $Cu_3Ca(OH)_6Cl_2 \cdot H_2O$, P–3m1 a = 6.6606(9), c = 5.8004(8) Å	tondiite (Malcherek et al., 2014) $Cu_3Mg(OH)_6Cl_2$, R–3m a = 6.8377(7), c = 14.088(2) Å
		KULIGINITE $Fe_3Mg(OH)_6Cl_2$, R–3** a = 6.9521(5), c = 14.5740(11) Å
		paratacamite (Welch et al., 2014) $Cu_6Cu_6(Zn,Cu)_3(Zn,Cu)(OH)_{24}Cl_8$, R–3*** a = 13.6440(4), c 14.0354(7) Å
		paratacamite-(Mg) (Kampf et al., 2013b) $Cu_6Cu_6(Mg,Cu)_3(Mg,Cu)(OH)_{24}Cl_8$, R–3*** a = 13.689(1), c = 14.025(1) Å
		paratacamite-(Ni) (Sciberras et al., 2013) $Cu_6Cu_6(Ni,Cu)_3(Ni,Cu)(OH)_{24}Cl_8$, R–3*** a = 13.682(2), c = 13.916(2) Å

This is a preprint, the final version is subject to change, of the American Mineralogist (MSA)
Cite as Authors (Year) Title. American Mineralogist, in press.
DOI: https://doi.org/10.2138/am-2018-6363

*Crystal structures of kempite and hibbingite have been never determined, so structural formulae are given by analogy with atacamite. Lattice parameters from original sources are transformed to the conventional setting ($a < b < c$).

**Pronounced $R\bar{3}m$ pseudosymmetry (see Crystal structure section)

***Pronounced herbertsmithite-like $R\bar{3}m$ substructure with $a_s = a/2$